

Inverse magnetic catalysis in the three-flavor NJL model with axial-vector interaction

Lang Yu,^{1,*} Jos Van Doorselaere,^{2,†} and Mei Huang^{1,3,‡}

¹*Institute of High Energy Physics, Chinese Academy of Sciences, Beijing 100049, China*

²*Laboratoire de Mathématiques et Physique Théorique, Université de Tours, 37000 Tours, France*

³*Theoretical Physics Center for Science Facilities, Chinese Academy of Sciences, Beijing 100049, China*

(Received 14 December 2014; published 6 April 2015)

In this paper we explore the chiral phase transition in QCD within the three-flavor Nambu–Jona-Lasinio model with a negative coupling constant in the isoscalar axial-vector channel, which is associated with a polarized instanton–anti-instanton molecule background. The QCD phase diagram described in this scenario shows a new first order phase transition around the transition temperature T_c toward a phase without chiral condensates, but with nontrivial dynamic chiral chemical potentials for the light quarks, spontaneously giving rise to local charge parity violation and local chirality imbalance. The corresponding critical temperature T_{5c} for this phase transition decreases with the magnetic field and it gives a natural explanation to the inverse magnetic catalysis effect for light quarks when incorporating a reasonable value of the coupling constant in the isoscalar axial-vector channel. Furthermore, when the isoscalar axial-vector interaction is dominant in the light quark sector and suppressed in the strange quark sector, it is found that there is no inverse magnetic catalysis for strange quark condensate, which agrees with lattice results.

DOI: 10.1103/PhysRevD.91.074011

PACS numbers: 12.38.Aw, 12.38.Mh

I. INTRODUCTION

Investigation of the QCD phase structure in the presence of strong external magnetic fields has become a major topic in both theoretical and experimental research into the physics of strongly interacting matter. This topic is of paramount importance to understand the phenomenology of noncentral heavy ion collisions at the Relativistic Heavy Ion Collider and the Large Hadron Collider (LHC), in which a strong magnetic field reaching up to $\sqrt{eB} \sim (0.1\text{--}1.0)$ GeV [1–4] can be generated. In addition, strong magnetic fields could also have existed in the strong and electroweak phase transition [5,6] of the early Universe, and they exist in compact stars like magnetars [7].

The breaking and restoration of chiral symmetry, which is described by the behavior of the quark condensate, is one of the most intriguing nonperturbative aspects of QCD. Therefore, it is of great interest to speculate on the effect of magnetic fields on the behavior of the chiral condensate in QCD at zero and finite temperatures. Since the 1990s, a related phenomenon known as magnetic catalysis has been recognized [8–11]. It refers to an enhancement of the quark condensate and thus an increase of the chiral transition temperature T_c under the magnetic field. This is agreed on by most of earlier low-energy effective models and approximations to QCD [8–10,12–23] as well as lattice QCD simulations [24–28] in the past twenty years. However, recently, a lattice group [29,30] revealed surprising results

that the transition temperature T_c decreases as a function of the external magnetic field, and the chiral condensate shows a nonmonotonic behavior as a function of the external magnetic field in the crossover region. This prediction is in contrast to the majority of previous calculations, and the partly decreasing behavior of the chiral condensate with the increasing B near T_c , causing a decreasing dependence of T_c on B , is called inverse magnetic catalysis. Moreover, it is concluded in Ref. [30] that the QCD system exhibits inverse magnetic catalysis for sufficiently small quark masses only (e.g., u and d quarks) and the strange quark never shows this effect at all temperatures.

There are several recent studies [31–43] discussing the origin of the phenomenon of the decreasing behavior of the chiral critical temperature with increasing B and the inverse magnetic catalysis around T_c . For example, the magnetic inhibition [31], the mass gap in the large N_c limit [32], the contribution of sea quarks [33], a running coupling parameter dependent on the magnetic field intensity and/or the temperature [36,37,42–44] and an antiscreening effect of the color charges for quarks [40,45], etc. are proposed to understand this puzzle. Particularly, a very natural and competitive mechanism attributes the inverse magnetic catalysis to the local chirality imbalance induced by the nontrivial topological gluon configuration, arising from a sphaleron transition [34] or the instanton–anti-instanton ($I\bar{I}$) molecule pairing [38].

As discussed in Ref. [38], the chirality imbalance, which is associated with the violation of the parity (\mathcal{P}) and charge parity (\mathcal{CP}) symmetry, is induced by the nonzero topological charge Q_T through the axial anomaly of QCD

*yulang@mail.ihep.ac.cn

†jvdoorss@gmail.com

‡huangm@mail.ihep.ac.cn

$$\Delta N_5 = \int d^4x \partial_\mu j_5^\mu = -2N_f Q_T, \quad (1)$$

where N_f is the number of flavors, $\Delta N_5 = N_5(t = +\infty) - N_5(t = -\infty)$, with $N_5 = N_R - N_L$ denoting the number difference between right- and left-hand quarks, and $j_5^\mu = \bar{\psi} \gamma^\mu \gamma^5 \psi$ denotes the isospin singlet axial-vector current. A consequence of this violation is the existence of two kinds of local domains with the same quantum numbers but opposite net topological charges, which will lead to the generation of local chirality imbalances but zero average chirality, as well as the local \mathcal{P} and \mathcal{CP} violation. The modification of the QCD phase diagram by the chirality imbalance has been studied in some references, [46–48]. Especially, the recent observation of charge azimuthal correlations at Relativistic Heavy Ion Collider and LHC [49–51] may be resulting from the chiral magnetic effect with local \mathcal{P} and \mathcal{CP} violation, which is an interesting combined effect of both the strong magnetic field and the nontrivial topological gluon configuration of the quark-gluon plasma. Based on the above discussions, the enhancement of the chirality imbalance by magnetic fields, which coincides with the lattice results in Ref. [52], will naturally result in a decreasing chiral critical temperature, since it destroys the pairing between the left-hand quark (antiquark) and the right-hand antiquark (quark).

In Ref. [38], a mechanism has been presented to generate local chirality imbalance based on the $\bar{I}\bar{I}$ molecule picture [53–57], which is regarded as one effective mechanism responsible for nonperturbative properties of QCD in the region $T \simeq T_c - 2T_c$ [55–57]. By using an unconventional repulsive isoscalar axial-vector interaction in a two-flavor Nambu-Jona-Lasinio (NJL) model [55], we find that a dynamical chiral chemical potential related to the local chirality imbalance is induced spontaneously at the temperatures near T_c . It is also found that the increasing magnetic field helps to lower the critical temperature due to the appearance of the local chirality. Moreover, since the local chirality imbalance can only be produced around T_c , it gives a reasonable explanation for why inverse magnetic catalysis only appears at the temperatures around T_c , while magnetic catalysis still occurs at zero and low temperatures.

However, the lattice result in Ref. [30] shows that the strange quark condensate does not exhibit inverse magnetic catalysis, but simply increases with magnetic field at all temperatures. In this paper, we extend our analysis and calculations to the $2 + 1$ flavors, and investigate the corresponding effects of the axial-vector interaction on both the local chirality imbalance and the chiral critical temperatures for u , d , and s quarks. The paper is organized as follows. In Sec. II, we give a general description of the $2 + 1$ -flavor NJL model and formalism by considering the repulsive axial-vector interactions stemming from the interacting $\bar{I}\bar{I}$ molecule model. In Sec. III, we discuss the

main results of the numerical calculations. Finally, our conclusions and perspectives are presented in Sec. IV.

II. MODEL AND FORMALISM

In this section, we present the three-flavor NJL model [58–67] by adding the vector and axial-vector interaction terms. The Lagrangian density of our model in the presence of an external magnetic field is given by

$$\mathcal{L} = \bar{\psi}(i\gamma_\mu D^\mu - \hat{m})\psi + \mathcal{L}_{\text{sym}} + \mathcal{L}_{\text{det}} - \mathcal{L}_{VA}, \quad (2)$$

where $\psi = (u, d, s)^T$ corresponds to the quark field of three flavors, and $\hat{m} = \text{diag}(m_u, m_d, m_s)$ is the corresponding current mass matrix. The covariant derivative, $D_\mu = \partial_\mu - iq_f A_\mu$, couples quarks to an external magnetic field $\mathbf{B} = (0, 0, B)$ along the positive z direction, via a background Abelian gauge field $A^\mu = (0, 0, Bx, 0)$. And q_f is defined as the electric charge of the quark field with flavor f . \mathcal{L}_{sym} and \mathcal{L}_{det} are given by

$$\mathcal{L}_{\text{sym}} = \frac{G_S}{2} \sum_{a=0}^8 [(\bar{\psi} \lambda^a \psi)^2 + (\bar{\psi} \lambda^a i\gamma^5 \psi)^2], \quad (3)$$

$$\mathcal{L}_{\text{det}} = -K \{ \det [\bar{\psi}(1 + \gamma^5)\psi] + \det [\bar{\psi}(1 - \gamma^5)\psi] \}, \quad (4)$$

where λ^a are the Gell-Mann matrices in flavor space ($\lambda^0 = \sqrt{2/3}I$) and the determinant is in flavor space also. The \mathcal{L}_{sym} term corresponds to the usual four-fermion interactions of scalar and pseudoscalar channels that respect $SU(3)_V \otimes SU(3)_A \otimes U(1)_V \otimes U(1)_A$ symmetry. The \mathcal{L}_{det} term corresponds to the 't Hooft six-fermion determinant interactions [68] that break $U(1)_A$ symmetry. As for the \mathcal{L}_{VA} term, it represents the four-fermion interactions of vector and axial-vector channels under the invariance of $SU(3)_V \otimes SU(3)_A \otimes U(1)_V \otimes U(1)_A$ symmetry. The last two terms are added to introduce chiral interactions, which are chosen such that they correspond to effective chirally asymmetric interactions with an instanton background.

The connection between instantons and chiral symmetry breaking is well known. Essentially it is a consequence of an index theorem that shows how a topologically nontrivial gauge configuration—the instanton—gives rise to an asymmetry in occupation of left and right chiral eigenmodes, observed through the existence of a fermion condensate. A feature of this index theorem is that all nontrivial physics happens in the zero-mode space. In a sense, the price we pay for those modes not to contribute to the action is the violation of chiral symmetry. At zero as well as low temperatures, the 't Hooft interaction is dominant; the random instantons play an important role in chiral symmetry breaking. However, at high temperatures and near the chiral phase transition, the instantons are no longer random, but become correlated. Therefore, it was suggested in

Refs. [53–55] that the growing correlations between instantons and anti-instantons near T_c will lead to the decrease of random instantons but the increase of instanton–anti-instanton molecule pairs. This means that the random instantons and anti-instantons are not annihilated but paired up into the correlated $I\bar{I}$ molecules when chiral phase transition happens. As shown in [55], in the temperature region of $T \gtrsim T_c$, the $I\bar{I}$ molecules pairing induces repulsive effective local four-quark interactions in the isoscalar axial-vector channel. This unconventional repulsive axial-vector interaction leads to a repulsive axial-vector mean field in the spacelike components but an attractive one in the timelike components, which naturally induces a spontaneous local \mathcal{CP} violation and local chirality imbalance as shown in [38].

In Refs. [38,55], the instanton background only couples to light u, d quarks, and the \mathcal{L}_{VA} in the isoscalar vector and axial vector takes the form of

$$\mathcal{L}_{VA}^{u,d} = \sum_{f=u,d} [G_V(\bar{\psi}_f \gamma^\mu \psi_f)^2 + G_A(\bar{\psi}_f \gamma^\mu \gamma^5 \psi_f)^2]. \quad (5)$$

We may generalize this term to the three-flavor case as follows:

$$\mathcal{L}_{VA}^{u,d,s} = \sum_{f=u,d,s} [G_V(\bar{\psi}_f \gamma^\mu \psi_f)^2 + G_A(\bar{\psi}_f \gamma^\mu \gamma^5 \psi_f)^2]. \quad (6)$$

In reality, considering the strange quark mass is heavier than light u, d quarks, the isoscalar vector and axial-vector interaction induced by instanton background might take the form in between Eqs. (5) and (6). For example, the quark propagator in a single instanton background is associated with the quark zero modes [68]

$$\psi_0^\pm(x) = \frac{\rho}{\pi(r^2 + \rho^2)^{3/2}} \frac{\not{x}}{r} U, \quad (7)$$

where the superscript \pm corresponds to an (anti-) instanton centered at x_0 and with size ρ . The spin-color matrix U satisfies $(\vec{\sigma} + \vec{\tau})U = 0$ and $r = x - x_0$. The zero-mode contributions will enter into the calculation of the correlators through the leading term in the spectral representation of the quark background field propagator

$$S_q^\pm(x, y) = \frac{\psi_0^\pm(x) \psi_0^{\pm\dagger}(y)}{m_q^*(\rho)} + O(\rho m_q^*). \quad (8)$$

Here, the flavor dependent effective quark mass $m_q^*(\rho) = m_q - \frac{2}{3} \pi^2 \rho^2 \langle \bar{q}q \rangle$ (where q stands for up, down, and strange quarks) in the denominator is generated by interactions with long-wavelength QCD vacuum fields as shown in Ref. [69]. It can be seen that the strange quark propagator in the instanton background is suppressed by $1/m_s^*$. Extending this to the instanton–anti-instanton molecule

background, we can assume the actual interaction in the isoscalar vector and axial-vector channel can be written as

$$\mathcal{L}_{VA} = \sum_{f=u,d} [G_V(\bar{\psi}_f \gamma^\mu \psi_f)^2 + G_A(\bar{\psi}_f \gamma^\mu \gamma^5 \psi_f)^2] + [G'_V(\bar{s} \gamma^\mu s)^2 + G'_A(\bar{s} \gamma^\mu \gamma^5 s)^2], \quad (9)$$

with $G'_V \ll G_V$ and $G'_A \ll G_A$ (G'_V/G_V or $G'_A/G_A \sim (m_u/m_s)^2$ in the chirally symmetric phase by Eq. (8), where m_u and m_s represent the current masses of u and s quarks, respectively). A compelling consequence of this argument is that the \mathcal{L}_{VA} -term, which is the essential source of the inverse magnetic catalysis in our approach, distinguishes between the isoscalar channel with light quarks and the one with strange quarks. It was found on the lattice QCD [30] that the inverse magnetic catalysis effect appears only for light quarks, not for strange quarks, an implicit feature in our approach. In the following calculations, we take two cases for the isoscalar vector and axial-vector interaction:

$$\text{Case I: take } \mathcal{L}_{VA}^{u,d} \quad (10)$$

$$\text{Case II: take } \mathcal{L}_{VA}^{u,d,s}. \quad (11)$$

Note that it has been discussed in Ref. [38] that G_S and G_V are expected to be positive at the whole temperature region [62,63,65,66] and are assumed to be keeping the constants fixed by the mesonic properties in QCD vacuum for simplicity, whereas G_A is expected to be positive at zero and low temperatures [62,63] and to be negative at the temperatures above T_c as a result of the interacting instanton–anti-instanton molecule model [53–55]. It has been shown in Ref. [55] that a negative G_A interaction induced by the correlated instanton–anti-instanton molecule pairs near T_c will give rise to nontrivial influence on the chiral phase transition. Therefore, we treat G_A as a free parameter in the NJL model of SU(3)-flavor version as we did in Ref. [38] with two light flavors. As discussed in Ref. [38], although it is a simple assumption to keep G_A negative in the entire temperature range, it has little influence on the final results since it shows the same numerical results as the calculations with positive G_A below T_c .

Working at the mean field level, one gets the thermodynamical potential per unit volume Ω by integrating out the quark fields ψ of the Lagrangian density of Eq. (2),

$$\Omega = \frac{1}{4G_S} \sum_{f=u,d,s} \sigma_f^2 + \frac{K}{2G_S^3} \sigma_u \sigma_d \sigma_s - \frac{\tilde{\mu}_5^2}{4G_A} + \sum_{f=u,d,s} \Omega^f, \quad (12)$$

where $\sigma_f = -2G_S \langle \bar{\psi}_f \psi_f \rangle$ ($f = u, d, s$) and

$$\begin{aligned}\tilde{\mu}_5 &= -2G_A \sum_{f=u,d} \langle \bar{\psi}_f \gamma^0 \gamma^5 \psi_f \rangle, \quad \text{for Case I,} \\ \tilde{\mu}_5 &= -2G_A \sum_{f=u,d,s} \langle \bar{\psi}_f \gamma^0 \gamma^5 \psi_f \rangle, \quad \text{for Case II.}\end{aligned}\quad (13)$$

The contributions from the fermion loop for each flavor are given by

$$\begin{aligned}\Omega^f &= -N_c \frac{|q_f B|}{2\pi} \sum_{s_z, k} \alpha_{s_z, k} \times \left[\int_{-\infty}^{\infty} \frac{dp_z}{2\pi} f_{\Lambda}^2(p) \omega_k^f(p) \right. \\ &\quad \left. + 2T \ln(1 + e^{-\omega_k^f/T}) \right],\end{aligned}\quad (14)$$

where

$$\omega_k^f = \begin{cases} \sqrt{M_f^2 + [|\mathbf{p}| + s_z \tilde{\mu}_5 \text{sgn}(p_z)]^2} & \text{for } f = u, d \\ \sqrt{M_f^2 + |\mathbf{p}|^2} & \text{for } f = s \end{cases}\quad (15)$$

are the dispersion relation for the thermal eigenfrequencies with spin factors $s_z = \pm 1$ for case I, and

$$\omega_k^f = \sqrt{M_f^2 + [|\mathbf{p}| + s_z \tilde{\mu}_5 \text{sgn}(p_z)]^2} \quad f = u, d, s \quad (16)$$

are the dispersion relation for the thermal eigenfrequencies with spin factors $s_z = \pm 1$ for case II. The gap equations for quark mass take the following form:

$$\begin{aligned}M_u &= m_u + \sigma_u + \frac{K}{2G_S^2} \sigma_s \sigma_d, \\ M_d &= m_d + \sigma_d + \frac{K}{2G_S^2} \sigma_s \sigma_u, \\ M_s &= m_s + \sigma_s + \frac{K}{2G_S^2} \sigma_u \sigma_d.\end{aligned}\quad (17)$$

The 3-momentum \mathbf{p} in a magnetic field is given by

$$\mathbf{p}^2 = p_z^2 + 2|q_f B|k, \quad (18)$$

and $k = 0, 1, 2, \dots$ is a non-negative integer number labeling the Landau levels. The spin degeneracy factor is expressed as

$$\alpha_{s_z, k} = \begin{cases} \delta_{s_z, +1} & \text{for } k = 0, qB > 0, \\ \delta_{s_z, -1} & \text{for } k = 0, qB < 0, \\ 1 & \text{for } k \neq 0. \end{cases}\quad (19)$$

Following Ref. [46] we use a smooth regularization form factor

$$f_{\Lambda}(p) = \sqrt{\frac{\Lambda^{2N}}{\Lambda^{2N} + |\mathbf{p}|^{2N}}}, \quad (20)$$

where we take $N = 5$. Now, by making use of Eq. (12), σ_f and $\tilde{\mu}_5$ can be determined self consistently as solutions to the saddle point equations

$$\frac{\partial \Omega}{\partial \sigma_f} = \frac{\partial \Omega}{\partial \tilde{\mu}_5} = 0. \quad (21)$$

Numerically one can obtain these solutions by a minimization and moreover find the true vacuum by looking at the global minimum. This will prove essential for our model which has multiple minima breaking chiral symmetry spontaneously.

The parameters of our model, the cutoff Λ , the coupling constants G_S and K , and the current quark masses $m_u = m_d$ and m_s are determined by fitting f_{π} , m_{π} , m_K , and $m_{\eta'}$ to their empirical values by using the smooth regularization method. We obtain $\Lambda = 604.5$ MeV, $m_u = m_d = 5.1$ MeV, $m_s = 133.0$ MeV, $G_S \Lambda^2 = 3.250$, and $K \Lambda^5 = 10.58$.

G_A will be treated as a free parameter, and we perform our calculations over a limited range of ratios,

$$r_A = G_A/G_S. \quad (22)$$

It is discussed in Ref. [38] that when $r_A \geq 0$ we always obtain the ordinary magnetic catalysis effect and only when $r_A < 0$ the inverse magnetic catalysis effect can be seen.

III. NUMERICAL RESULTS AND DISCUSSION

Considering the interaction in the strange quark channel is suppressed, for our numerical calculations, we mostly take the isoscalar axial-vector interaction of case I, i.e., take the form in Eq. (5).

We study the chiral phase transition at finite temperature by using Eq. (21) for several different values of the parameters r_A and eB , representing different intensity for the instanton–anti-instanton molecule background and the magnetic field background, respectively. Consequently, the diagrams of $\sigma - T$ for different quark flavors as well as the diagrams of $\tilde{\mu}_5 - T$ can be obtained, which allow us to efficiently find the transition temperatures as functions of the parameters r_A and eB . Actually, each of the condensates thus has its own specific transition temperature, which is defined by the temperature at the inflection point of the $\sigma - T$ diagram for each flavor, i.e., the maximum point of the quantity $\partial\sigma/\partial T$. Here, we use $\sigma_u + \sigma_d$ to determine the transition temperature T_c for the chiral phase transition of QCD.

In Fig. 1, we display the quark condensates of σ_u , σ_d , and σ_s as well as dynamical chiral chemical potential $\tilde{\mu}_5$ as

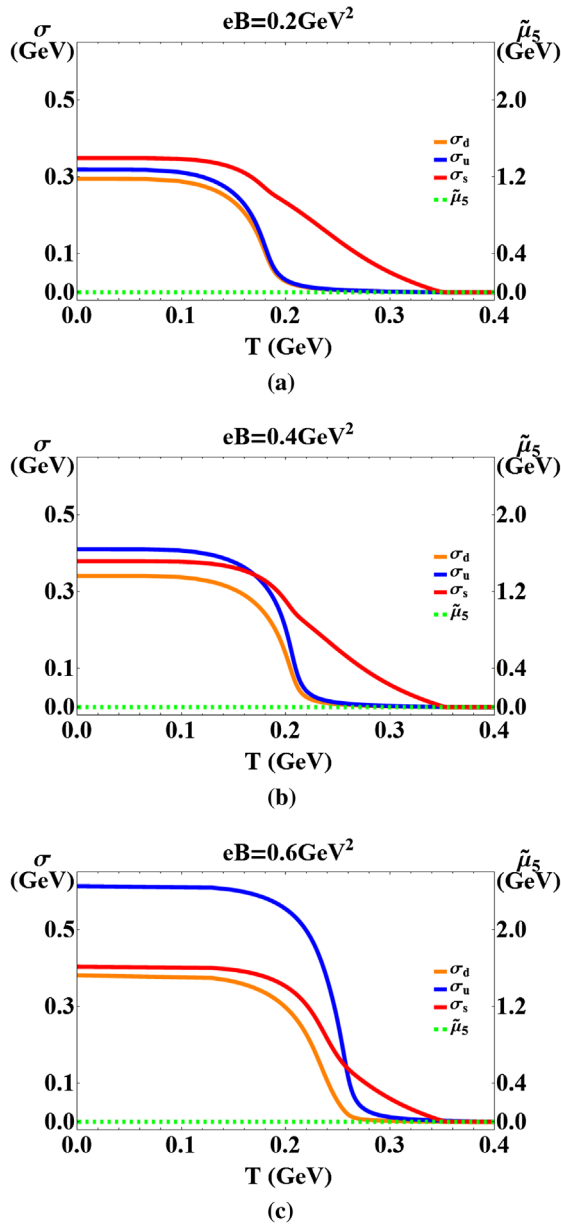


FIG. 1 (color online). The quark condensate σ_f ($f = u, d, s$) and dynamical chiral chemical potential $\tilde{\mu}_5$ as a function of T at $r_A = 0$ for several different values of eB . (a) σ_f and $\tilde{\mu}_5$ for $eB = 0.2 \text{ GeV}^2$ at $r_A = 0$. (b) σ_f and $\tilde{\mu}_5$ for $eB = 0.4 \text{ GeV}^2$ at $r_A = 0$. (c) σ_f and $\tilde{\mu}_5$ for $eB = 0.6 \text{ GeV}^2$ at $r_A = 0$.

functions of T for several different values of eB without considering additional axial-vector couplings, i.e., $r_A = 0$ and $\tilde{\mu}_5 \equiv 0$, and the ordinary magnetic catalysis effect can be exactly found from the plots. It is apparent that the light quark condensates $\langle \bar{u}u \rangle$ and $\langle \bar{d}d \rangle$ show different behavior in the presence of the magnetic field because of their different electric charges. In fact, even if we choose positive values for the parameter r_A , fitted by the conventional SU(3)-flavor NJL model, we will acquire the same results. This is because of the fact that when $r_A > 0$, the potential

energy density Ω can only have a local maximum at nonzero $\tilde{\mu}_5$, which forces $\langle \bar{\psi} \gamma^0 \gamma^5 \psi \rangle$ to be zero so that $\tilde{\mu}_5 = 0$ accordingly. In this way the quark condensates are independent of G_A , which is a consequence of the Vafa-Witten theorem [70].

Next, as discussed in Ref. [38], by switching on a negative r_A , we introduce a nontrivial dependence of the thermodynamical potential Ω on the dynamic chiral chemical potential $\tilde{\mu}_5$, which adds an extra dimension to the mean field surface of Ω . As is shown in Fig. 2, there are two local minima for the potential Ω . When the temperature is low, the original local minimum representing nonzero quark condensates is dominant, since it is the global minimum. However, sufficient heating of the QCD system makes the local minimum for nontrivial $\tilde{\mu}_5$ energetically more favorable while the chiral condensates are weakened to the trivial state. As a result, the vacuum tunnels to a state with local chirality imbalance between right- and left-hand quarks as this metastable state becomes the new global minimum. It is important to point out that the potential Ω in Eq. (12) is even in $\tilde{\mu}_5$ so one can get separated local domains with chiral densities of both signs. Moreover, another important consequence of the competition between these two local minima is that no “mixed” state appears, so one has either nonzero quark condensates but no chirality imbalance or an instability towards the formation of nonzero dynamic chiral chemical potential but no presence of condensates. This is clear from the fact that the minima in Fig. 2 appear on either of the axes and are a consistent feature of all our simulations.

In fact, the magnitude of the unconventional negative G_A , which leads to an attractive mean field in the timelike components of the axial-vector channel, reflects the coupling strength of the attraction for $\tilde{\mu}_5$. In Figs. 3–5, we compare our numerical results of quark condensates σ_f ($f = u, d$, and s) and dynamic chiral chemical potential $\tilde{\mu}_5$ as functions of T for several magnetic fields at $r_A = -0.3, -0.5$, and -0.7 . One can distinguish two distinct cases as a result of the magnitude of negative r_A : (i) $T_c(eB = 0; r_A = 0) < T_{5c}(eB = 0)$ and (ii) $T_c(eB = 0; r_A = 0) > T_{5c}(eB = 0)$.

If the magnitude of G_A is small, approximately $-0.5 < r_A < 0$ for our model, it is easy to find that we are in case (i), i.e., $T_{5c} > T_c(r_A = 0)$ at $eB = 0$. For example, as shown by Fig. 3 of $r_A = -0.3$ and Fig. 4 of $r_A = -0.5$, when the external magnetic field is not strong enough, the ordinary phase transition into the chirally restored phase takes place at a lower temperature and is the dominant effect in destroying the quark condensates, whereas a local \mathcal{CP} -odd first order phase transition for $\tilde{\mu}_5$ is spontaneously generated at a higher critical temperature $T_{5c} > T_c$. As the magnetic field grows, both critical temperatures, T_{5c} and T_c , approach each other and two local minima in the thermodynamic potential Ω coexist like in the example of Fig. 2. At some critical value of magnetic

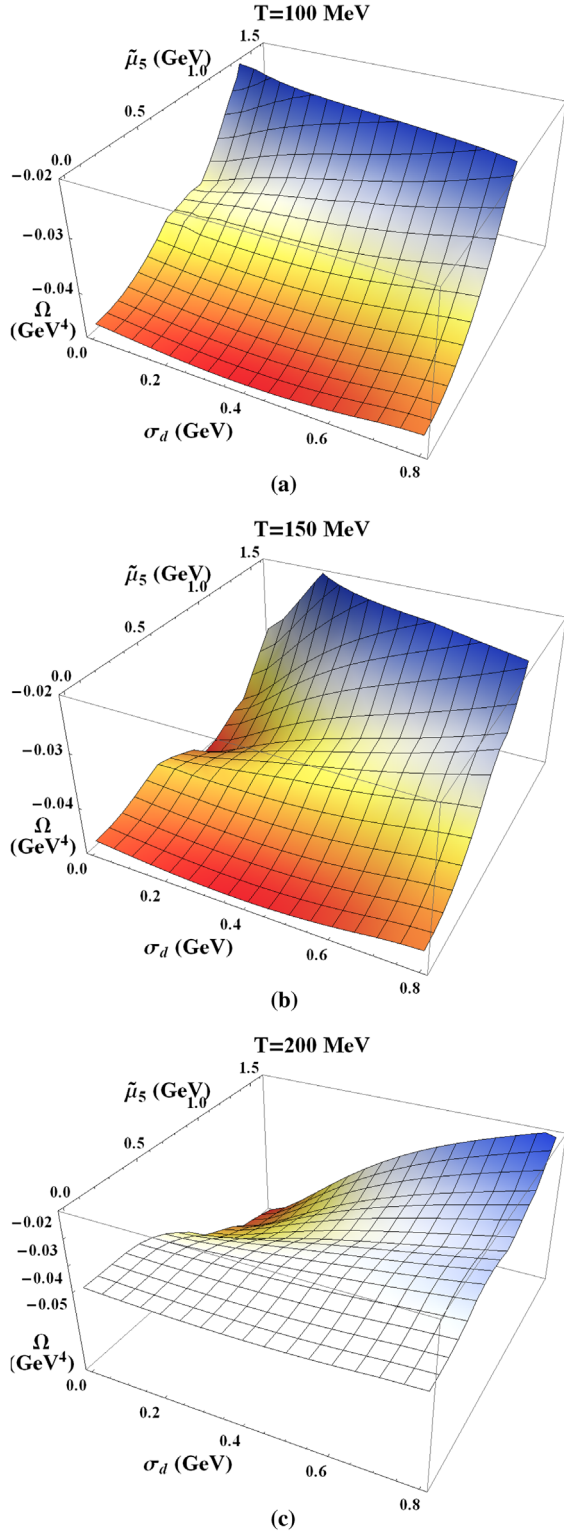


FIG. 2 (color online). A two-dimensional minimal surface of the potential Ω for case I as a function of σ_d and $\tilde{\mu}_5$ at $r_A = -0.5$ and $eB = 0.6 \text{ GeV}^2$ for several different values of temperature. (a) Ω at $r_A = -0.5$ and $eB = 0.6 \text{ GeV}^2$ for $T = 100 \text{ MeV}$ (below T_c). (b) Ω at $r_A = -0.5$ and $eB = 0.6 \text{ GeV}^2$ for $T = 150 \text{ MeV}$ (around T_c). (c) Ω at $r_A = -0.5$ and $eB = 0.6 \text{ GeV}^2$ for $T = 200 \text{ MeV}$ (above T_c).

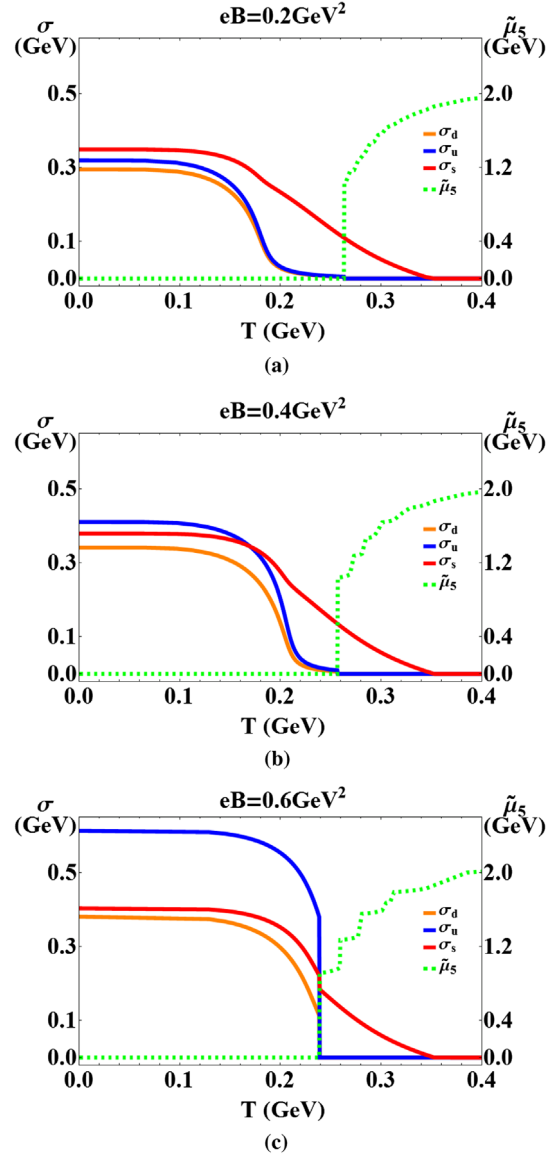


FIG. 3 (color online). For case I, the quark condensate σ_f ($f = u, d, s$) and dynamical chiral chemical potential $\tilde{\mu}_5$ as a function of T at $r_A = -0.3$ for several different values of eB . (a) σ_f and $\tilde{\mu}_5$ for $eB = 0.2 \text{ GeV}^2$ at $r_A = -0.3$. (b) σ_f and $\tilde{\mu}_5$ for $eB = 0.4 \text{ GeV}^2$ at $r_A = -0.3$. (c) σ_f and $\tilde{\mu}_5$ for $eB = 0.6 \text{ GeV}^2$ at $r_A = -0.3$.

field B_c for a given r_A , these two critical temperatures meet each other and the first order transition for nonzero dynamical chiral chemical potential $\tilde{\mu}_5$ becomes the dominant effect, which makes σ_u and σ_d drop to zero at $T_c = T_{5c}$. Therefore, we find that, for u and d quarks in case (i), the critical temperature T_{5c} decreases with eB , while T_c increases at first and then decreases as the magnetic field grows. As for s quark condensate, it shows a slight jump because of $\tilde{\mu}_5$ background and then continues to dissolve with increasing temperature. The critical temperature $T_c(\sigma_s)$ will increase with eB always,

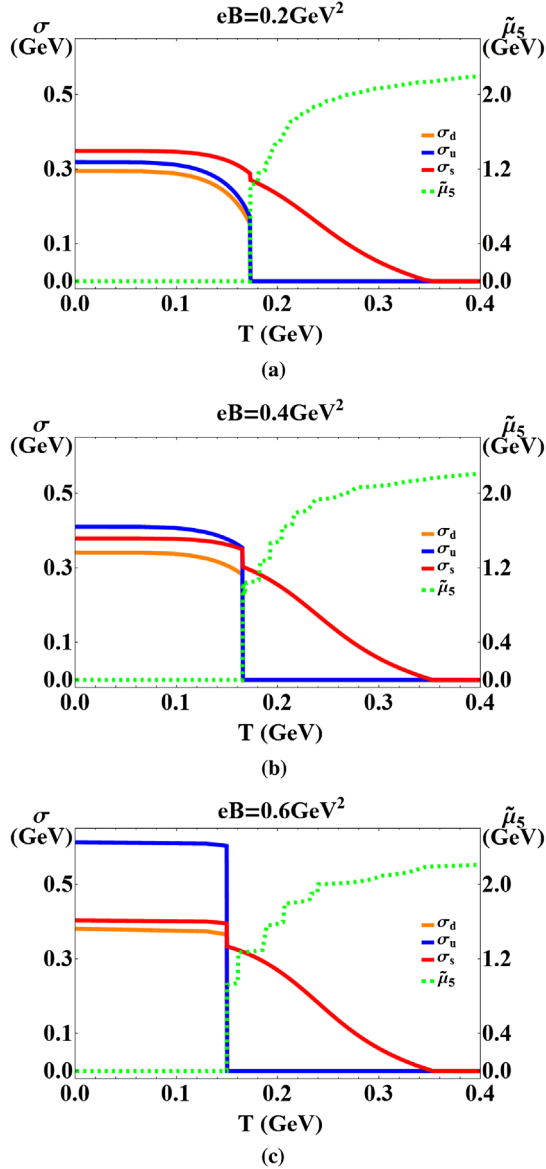


FIG. 4 (color online). For case I, the quark condensate σ_f ($f = f = u, d, s$) and dynamical chiral chemical potential $\tilde{\mu}_5$ as a function of T at $r_A = -0.5$ for several different values of eB . (a) σ_f and $\tilde{\mu}_5$ for $eB = 0.2 \text{ GeV}^2$ at $r_A = -0.5$. (b) σ_f and $\tilde{\mu}_5$ for $eB = 0.4 \text{ GeV}^2$ at $r_A = -0.5$. (c) σ_f and $\tilde{\mu}_5$ for $eB = 0.6 \text{ GeV}^2$ at $r_A = -0.5$.

depicted by Fig. 6, which is consistent with the lattice results in Ref. [30] in some sense.

If the magnitude of G_A is large enough ($r_A < -0.5$), that is, in case (ii), the light quark condensates are destroyed at $T_c = T_{5c}$ because the QCD ground state with chirality imbalanced density becomes more favorable around the critical temperature for any values of eB , before σ_u and σ_d are dissolved at their original critical temperature T_c without considering $\tilde{\mu}_5$, e.g., shown by Fig. 5 at $r_A = -0.7$. Hence, the critical temperatures T_c and T_{5c} for u and d quark condensates decrease with eB starting

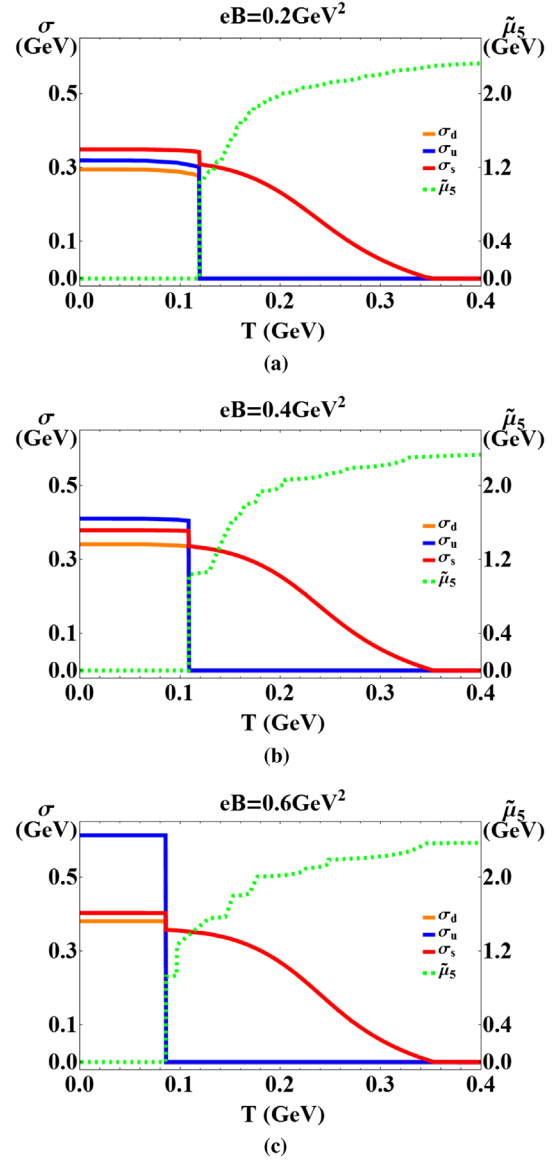


FIG. 5 (color online). For case I, the quark condensate σ_f ($f = u, d, s$) and dynamical chiral chemical potential $\tilde{\mu}_5$ as a function of T at $r_A = -0.7$ for several different values of eB . (a) σ_f and $\tilde{\mu}_5$ for $eB = 0.2 \text{ GeV}^2$ at $r_A = -0.7$. (b) σ_f and $\tilde{\mu}_5$ for $eB = 0.4 \text{ GeV}^2$ at $r_A = -0.7$. (c) σ_f and $\tilde{\mu}_5$ for $eB = 0.6 \text{ GeV}^2$ at $r_A = -0.7$.

from $eB = 0$, which is just the decreasing T_c dependence on B predicted by Ref. [29]. On the other hand, the condensates σ_u and σ_d increase with the magnetic field at zero and low temperatures still, which is the ordinary magnetic catalysis effect validated in Ref. [30]. The behavior of both strange quark condensate σ_s and the critical temperature $T_c(\sigma_s)$ is similar to that in case (i).

We can now put the data about the critical temperatures obtained from Figs. 3–5 into one $T_c - eB$ phase diagram of QCD. Adding more data points from identical simulations with other values of the background parameters r_A and eB ,

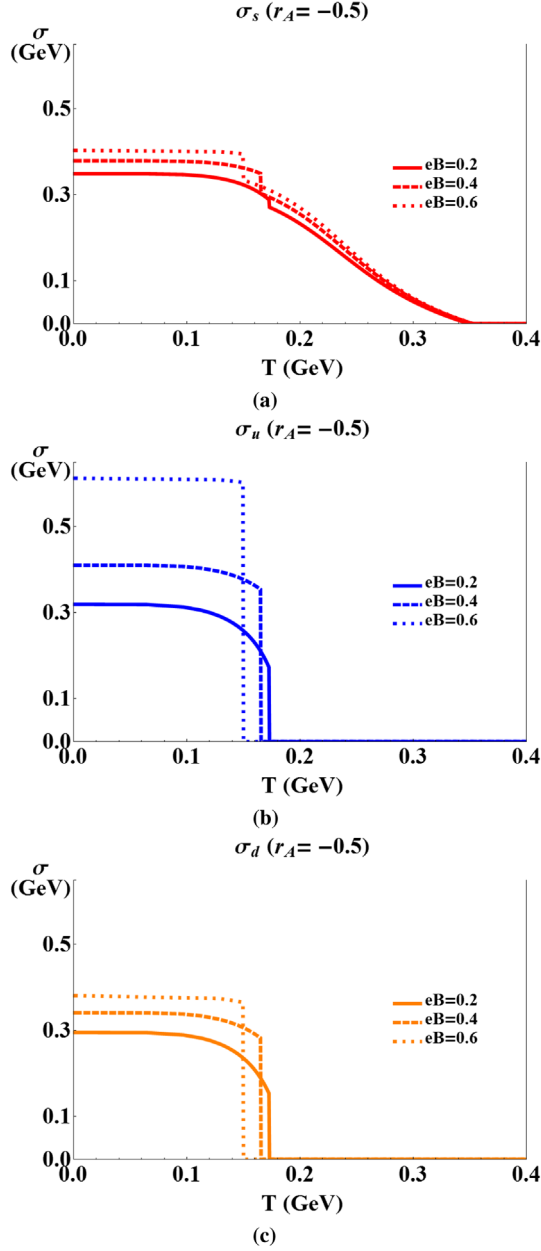


FIG. 6 (color online). For case I, the quark condensates σ_s , σ_u , and σ_d as a function of T at $r_A = -0.5$ for several different values of eB . (a) σ_s at $r_A = -0.5$ for several different values of eB . (b) σ_u at $r_A = -0.5$ for several different values of eB . (c) σ_d at $r_A = -0.5$ for several different values of eB .

we can find that the middle diagram of Fig. 7 shows two different possible types of dependence of T_c on the magnetic field as a result of the free parameter r_A , which has been discussed explicitly above. As a consequence, a reasonable strength of r_A , approximately between -0.5 and -0.55 by the simulations of our model, will naturally explain the decreasing dependence of T_c on eB obtained in a recent lattice QCD study [29]. If the magnitude of r_A is too small, less than 0.5, we cannot find a monotonously decreasing dependence of T_c on eB ; if the magnitude of r_A

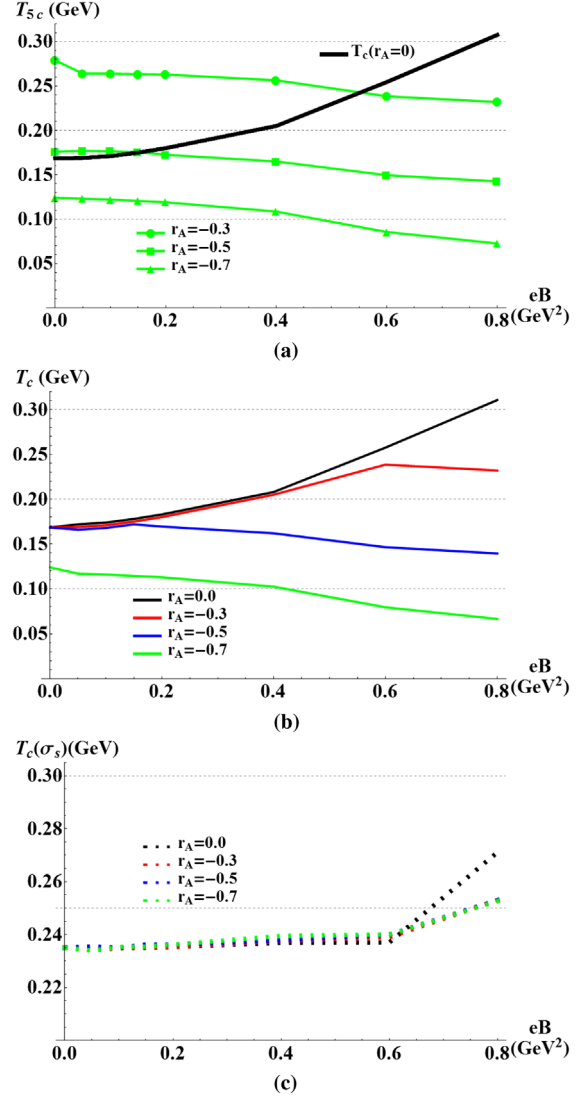


FIG. 7 (color online). (a) The critical temperature T_{5c} as a function of eB for several different values of r_A , comparing with T_c as a function of eB at $r_A = 0$. (b) The critical temperature T_c as a function of eB for several different values of r_A . (c) The critical temperature $T_c(\sigma_s)$ as a function of eB for several different values of r_A . The results are for case I.

is too big, more than 0.55, the value of T_c at $eB = 0$ will deviate from the lattice QCD result greatly. Furthermore, we can distinguish case (i) and case (ii) easily by the $T_{5c}(B)$ function from the top diagram of Fig. 7, the separation given by the thick black line for the critical temperature T_c at $r_A = 0$. As for the critical temperature $T_c(\sigma_s)$, depicted by the bottom diagram of Fig. 7, one can find that its behavior at different negative values of r_A is similar to that at $r_A = 0$, showing a slightly increasing dependence on eB .

The above calculations are based on case I, where the isoscalar axial-vector interaction only involves light u, d quarks. The isoscalar nature of the interaction \mathcal{L}_{VA} is essential for the nature of the phase transition. With little

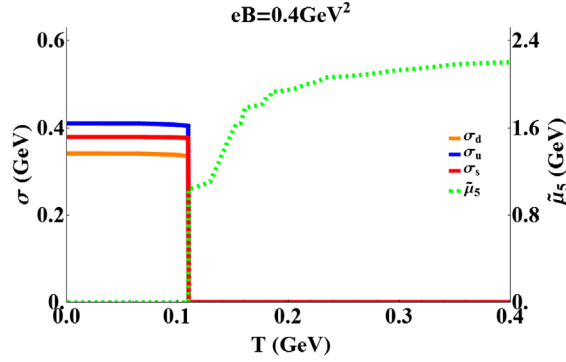


FIG. 8 (color online). For case II, the quark condensate σ_f ($f = u, d, s$) and dynamical chiral chemical potential $\tilde{\mu}_5$ as a function of T at $r_A = -0.5$ and $eB = 0.4 \text{ GeV}^2$ when introducing a negative axial-vector coupling to all three flavor quarks equally.

extra effort we were able to simulate case II where the four-fermion chiral attraction treats all flavors equally as given by Eq. (6). It can be seen that the results of σ_u and σ_d are very similar to what we found before, but rather than a small shift in the value of the heavy strange quark condensate, σ_s undergoes the same first order phase transition as the other two light flavors and vanishes at the transition temperature T_{5c} , as shown in Fig. 8. As we argued in the previous section, this kind of equal coupling with negative G_A to all three quark flavors is not to be expected for an axial-vector coupling induced by an instanton–anti-instanton molecule background, and not surprisingly, it does not reproduce the qualitative lattice result.

Before drawing our final conclusions, it is important to realize we can only trust our results qualitatively. Since the new minimum and the corresponding phase transition shown in Fig. 2 are in fact at a scale well beyond the cutoff of our theory, exact quantitative prediction is beyond the scope of the NJL framework. Qualitatively, however, we can be sure that the instability will emerge, and a new vacuum state will appear that is more favored than the chiral condensate when increasing magnetic fields around T_c and will thus give rise to the inverse magnetic catalysis effect. In that sense we think that our model is a good representation of the effect of instanton–anti-instanton molecule background on the chiral condensates, but we cannot produce accurate predictions for the large chiral densities involved.

IV. CONCLUSIONS

In this paper we extend our study to the QCD phase diagram as well as the behavior of quark condensates at finite temperature under an external magnetic field within the three-flavor NJL model including additional isoscalar vector and axial-vector channels. Note that an important and unconventional feature of our model is the isoscalar

axial-vector interaction with a negative coupling constant depending mostly on the up and down quarks, while the interaction in the strange quark sector is suppressed due to its heavier mass, which can be derived from the instanton–anti-instanton molecule model [55].

In this scenario, we have shown that a new way of destroying chiral condensates appears around T_c , replacing them by dynamical chiral chemical potential $\tilde{\mu}_5$ in a first order phase transition, which corresponds to a spontaneous generation of local \mathcal{P} and \mathcal{CP} violation and local chirality imbalance. Moreover, the critical temperature of this first order phase transition shows inverse magnetic catalysis, meaning that it decreases with increasing magnetic field.

The dominant features of the phase transition with respect to destroying the light quark condensates depend on the parameters of the model, a tunable axial-vector coupling constant G_A , and the background magnetic field B . When increasing the magnitude of G_A , we can find that it will decrease the critical temperature for the first order phase transition of $\tilde{\mu}_5$. And the increase of the magnetic field at a given G_A will also decrease the critical temperature T_{5c} . It means that, in the generic case, the increase of the magnitude of both parameters, G_A and eB , will catalyze the appearance of the local chirality imbalance. Therefore, with a reasonable value of G_A , making the ordinary chiral phase transition meet with the newly found first order phase transition at $eB = 0$ (however, this is not in agreement with previous lattice results at finite temperature, and possible reasons are discussed in Ref. [38]), the inverse magnetic catalysis effect can be naturally explained and a phase diagram is reproduced in Fig. 7, consistent with lattice QCD results [29].

On the other hand, since the lattice results of Ref. [30] indicated that strange quark condensate experience magnetic catalysis only, we investigate the behavior of strange quark condensate in our model also. When we introduce a negative axial-vector interaction channel including light quark currents only, it is found that the critical temperature $T_c(\sigma_s)$ exhibits little modification as a result of the instanton–anti-instanton molecule background, in some sense consistent with lattice results, although the strange condensate shows a slight jump arising from the appearance of $\tilde{\mu}_5$ in the $\sigma - T$ diagrams. This might be improved by considering the spatial structure of the topological density distribution, which is one of our future plans. In reality, the interaction in the isoscalar vector and axial-vector channel might look like Eq. (9), with a dominant isoscalar axial-vector interaction in the light quark sector and with a suppressed interaction in the strange quark sector. In this case, if the interaction in the strange sector is small enough, the result of chiral phase transitions will be the same as that in case I, and we can get the inverse magnetic catalysis for light quark condensates but magnetic catalysis for strange quark condensates around critical temperature, which is in agreement with lattice results.

ACKNOWLEDGMENTS

We thank M. Chernodub, J. Y. Chao, and I. Shovkovy for valuable discussions. This work is supported by the National Science Foundation of China (NSFC) under Grants No. 11275213 and No. 11261130311 (CRC 110 by DFG and NSFC), CAS key project under Grant

No. KJCX2-EW-N01, and the Youth Innovation Promotion Association of CAS. L. Y. is partially supported by the China Postdoctoral Science Foundation under Grant No. 2014M550841. The work of J. V. D. was supported by a grant from La Region Centre (France) and the Chinese-French Cai Yuanpei 2013 grant.

-
- [1] V. Skokov, A. Y. Illarionov, and V. Toneev, Estimate of the magnetic field strength in heavy-ion collisions, *Int. J. Mod. Phys. A* **24**, 5925 (2009).
- [2] V. Voronyuk, V. D. Toneev, W. Cassing, E. L. Bratkovskaya, V. P. Konchakovski, and S. A. Voloshin, (Electro-) magnetic field evolution in relativistic heavy-ion collisions, *Phys. Rev. C* **83**, 054911 (2011).
- [3] A. Bzdak and V. Skokov, Event-by-event fluctuations of magnetic and electric fields in heavy-ion collisions, *Phys. Lett. B* **710**, 171 (2012).
- [4] W.-T. Deng and X.-G. Huang, Event-by-event generation of electromagnetic fields in heavy-ion collisions, *Phys. Rev. C* **85**, 044907 (2012).
- [5] T. Vachaspati, Magnetic fields from cosmological phase transitions, *Phys. Lett. B* **265**, 258 (1991).
- [6] K. Enqvist and P. Olesen, On primordial magnetic fields of electroweak origin, *Phys. Lett. B* **319**, 178 (1993).
- [7] R. C. Duncan and C. Thompson, Formation of very strongly magnetized neutron stars—implications for gamma-ray bursts, *Astrophys. J.* **392**, L9 (1992).
- [8] S. P. Klevansky and R. H. Lemmer, Chiral symmetry restoration in the Nambu-Jona-Lasinio model with a constant electromagnetic field, *Phys. Rev. D* **39**, 3478 (1989).
- [9] K. G. Klimenko, *Teor. Mat. Fiz.* **89**, 211 (1991) [Three-dimensional Gross-Neveu model in an external magnetic field, *Theor. Math. Phys.* **89**, 1161 (1991)].
- [10] V. P. Gusynin, V. A. Miransky, and I. A. Shovkovy, Dimensional reduction and catalysis of dynamical symmetry breaking by a magnetic field, *Nucl. Phys. B* **462**, 249 (1996).
- [11] I. A. Shovkovy, Magnetic catalysis: a review, *Lect. Notes Phys.* **871**, 13 (2013).
- [12] I. A. Shushpanov and A. V. Smilga, Quark condensate in a magnetic field, *Phys. Lett. B* **402**, 351 (1997).
- [13] N. O. Agasian and I. A. Shushpanov, The quark and gluon condensates and low-energy QCD theorems in a magnetic field, *Phys. Lett. B* **472**, 143 (2000).
- [14] J. Alexandre, K. Farakos, and G. Koutsoumbas, Magnetic catalysis in QED(3) at finite temperature: beyond the constant mass approximation, *Phys. Rev. D* **63**, 065015 (2001).
- [15] N. O. Agasian, *Yad. Fiz.* **64**, 608 (2001) [Chiral thermodynamics in a magnetic field, *Phys. Atom. Nucl.* **64**, 554 (2001)].
- [16] T. D. Cohen, D. A. McGady, and E. S. Werbos, The chiral condensate in a constant electromagnetic field, *Phys. Rev. C* **76**, 055201 (2007).
- [17] R. Gatto and M. Ruggieri, Dressed Polyakov loop and phase diagram of hot quark matter under magnetic field, *Phys. Rev. D* **82**, 054027 (2010).
- [18] R. Gatto and M. Ruggieri, Deconfinement and chiral symmetry restoration in a strong magnetic background, *Phys. Rev. D* **83**, 034016 (2011).
- [19] A. J. Mizher, M. N. Chernodub, and E. S. Fraga, Phase diagram of hot QCD in an external magnetic field: possible splitting of deconfinement and chiral transitions, *Phys. Rev. D* **82**, 105016 (2010).
- [20] K. Kashiwa, Entanglement between chiral and deconfinement transitions under strong uniform magnetic background field, *Phys. Rev. D* **83**, 117901 (2011).
- [21] S. S. Avancini, D. P. Menezes, M. B. Pinto, and C. Providencia, The QCD critical end point under strong magnetic fields, *Phys. Rev. D* **85**, 091901 (2012).
- [22] J. O. Andersen, Thermal pions in a magnetic background, *Phys. Rev. D* **86**, 025020 (2012).
- [23] D. D. Scherer and H. Gies, Renormalization group study of magnetic catalysis in the three-dimensional Gross-Neveu model, *Phys. Rev. B* **85**, 195417 (2012).
- [24] P. V. Buividovich, M. N. Chernodub, E. V. Luschevskaya, and M. I. Polikarpov, Numerical study of chiral symmetry breaking in non-Abelian gauge theory with background magnetic field, *Phys. Lett. B* **682**, 484 (2010).
- [25] V. V. Braguta, P. V. Buividovich, T. Kalaydzhyan, S. V. Kuznetsov, and M. I. Polikarpov, The chiral magnetic effect and chiral symmetry breaking in SU(3) quenched lattice gauge theory, *Phys. At. Nucl.* **75**, 488 (2012).
- [26] M. D'Elia, S. Mukherjee, and F. Sanfilippo, QCD phase transition in a strong magnetic background, *Phys. Rev. D* **82**, 051501 (2010).
- [27] M. D'Elia and F. Negro, Chiral properties of strong interactions in a magnetic background, *Phys. Rev. D* **83**, 114028 (2011).
- [28] E.-M. Ilgenfritz, M. Kalinowski, M. Muller-Preussker, B. Petersson, and A. Schreiber, Two-color QCD with staggered fermions at finite temperature under the influence of a magnetic field, *Phys. Rev. D* **85**, 114504 (2012).
- [29] G. S. Bali, F. Bruckmann, G. Endrodi, Z. Fodor, S. D. Katz, S. Krieg, A. Schafer, and K. K. Szabo, The QCD phase diagram for external magnetic fields, *J. High Energy Phys.* **02** (2012) 044.
- [30] G. S. Bali, F. Bruckmann, G. Endrodi, Z. Fodor, S. D. Katz, and A. Schafer, QCD quark condensate in external magnetic fields, *Phys. Rev. D* **86**, 071502 (2012).

- [31] K. Fukushima and Y. Hidaka, Magnetic Catalysis vs Magnetic Inhibition, *Phys. Rev. Lett.* **110**, 031601 (2013).
- [32] T. Kojo and N. Su, The quark mass gap in a magnetic field, *Phys. Lett. B* **720**, 192 (2013).
- [33] F. Bruckmann, G. Endrodi, and T. G. Kovacs, Inverse magnetic catalysis and the Polyakov loop, *J. High Energy Phys.* **04** (2013) 112.
- [34] J. Chao, P. Chu, and M. Huang, Inverse magnetic catalysis induced by sphalerons, *Phys. Rev. D* **88**, 054009 (2013).
- [35] E. S. Fraga, B. W. Mintz, and J. Schaffner-Bielich, A search for inverse magnetic catalysis in thermal quark-meson models, *Phys. Lett. B* **731**, 154 (2014).
- [36] M. Ferreira, P. Costa, O. Lourenço, T. Frederico, and C. Providência, Inverse magnetic catalysis in the (2 + 1)-flavor Nambu-Jona-Lasinio and Polyakov–Nambu-Jona-Lasinio models, *Phys. Rev. D* **89**, 116011 (2014).
- [37] R. L. S. Farias, K. P. Gomes, G. I. Krein, and M. B. Pinto, Importance of asymptotic freedom for the pseudocritical temperature in magnetized quark matter, *Phys. Rev. C* **90**, 025203 (2014).
- [38] L. Yu, H. Liu, and M. Huang, Spontaneous generation of local CP violation and inverse magnetic catalysis, *Phys. Rev. D* **90**, 074009 (2014).
- [39] J. O. Andersen, W. R. Naylor, and A. Tranberg, Inverse magnetic catalysis and regularization in the quark-meson model, *J. High Energy Phys.* **02** (2015) 042.
- [40] E. J. Ferrer, V. de la Incera, and X. J. Wen, Quark anti-screening at strong magnetic field and inverse magnetic catalysis, *Phys. Rev. D* **91**, 054006 (2015).
- [41] B. Feng, D. Hou, and H. c. Ren, (Inverse) magnetic catalysis in Bose-Einstein condensation of neutral bound pairs, [arXiv:1412.1647](https://arxiv.org/abs/1412.1647).
- [42] A. Ayala, M. Loewe, A. J. Mizher, and R. Zamora, Inverse magnetic catalysis for the chiral transition induced by thermomagnetic effects on the coupling constant, *Phys. Rev. D* **90**, 036001 (2014).
- [43] A. Ayala, M. Loewe, and R. Zamora, Inverse magnetic catalysis in the linear sigma model with quarks, *Phys. Rev. D* **91**, 016002 (2015).
- [44] A. Ayala, J. J. Cobos-Martinez, M. Loewe, M. E. Tejeda-Yeomans, and R. Zamora, Finite temperature quark-gluon vertex with a magnetic field in the hard thermal loop approximation, *Phys. Rev. D* **91**, 016007 (2015).
- [45] E. J. Ferrer, V. de la Incera, I. Portillo, and M. Quiroz, New look at the QCD ground state in a magnetic field, *Phys. Rev. D* **89**, 085034 (2014).
- [46] K. Fukushima, M. Ruggieri, and R. Gatto, Chiral magnetic effect in the PNJL model, *Phys. Rev. D* **81**, 114031 (2010).
- [47] M. N. Chernodub and A. S. Nedelin, Phase diagram of chirally imbalanced QCD matter, *Phys. Rev. D* **83**, 105008 (2011).
- [48] R. Gatto and M. Ruggieri, Hot quark matter with an axial chemical potential, *Phys. Rev. D* **85**, 054013 (2012).
- [49] B. I. Abelev *et al.* (STAR Collaboration), Azimuthal Charged-Particle Correlations and Possible Local Strong Parity Violation, *Phys. Rev. Lett.* **103**, 251601 (2009).
- [50] B. I. Abelev *et al.* (STAR Collaboration), Observation of charge-dependent azimuthal correlations and possible local strong parity violation in heavy-ion collisions, *Phys. Rev. C* **81**, 054908 (2010).
- [51] B. Abelev *et al.* (ALICE Collaboration), Charge Separation Relative to the Reaction Plane in Pb-Pb Collisions at $\sqrt{s_{NN}} = 2.76$ TeV, *Phys. Rev. Lett.* **110**, 012301 (2013).
- [52] P. V. Buividovich, M. N. Chernodub, E. V. Luschevskaya, and M. I. Polikarpov, Numerical evidence of chiral magnetic effect in lattice gauge theory, *Phys. Rev. D* **80**, 054503 (2009).
- [53] E.-M. Ilgenfritz and E. V. Shuryak, Chiral symmetry restoration at finite temperature in the instanton liquid, *Nucl. Phys.* **B319**, 511 (1989).
- [54] E.-M. Ilgenfritz and E. V. Shuryak, Quark induced correlations between instantons drive the chiral phase transition, *Phys. Lett. B* **325**, 263 (1994).
- [55] T. Schafer, E. V. Shuryak, and J. J. M. Verbaarschot, The chiral phase transition and instanton—anti-instanton molecules, *Phys. Rev. D* **51**, 1267 (1995).
- [56] T. Schafer and E. V. Shuryak, Instantons in QCD, *Rev. Mod. Phys.* **70**, 323 (1998).
- [57] Z. Zhang, Correction to the chiral magnetic effect from axial-vector interaction, *Phys. Rev. D* **85**, 114028 (2012).
- [58] Y. Nambu and G. Jona-Lasinio, Dynamical model of elementary particles based on an analogy with superconductivity. I, *Phys. Rev.* **122**, 345 (1961).
- [59] Y. Nambu and G. Jona-Lasinio, Dynamical model of elementary particles based on an analogy with superconductivity. II, *Phys. Rev.* **124**, 246 (1961).
- [60] V. Bernard, R. L. Jaffe, and U. G. Meissner, Flavor mixing via dynamical chiral symmetry breaking, *Phys. Lett. B* **198**, 92 (1987).
- [61] V. Bernard, R. L. Jaffe, and U. G. Meissner, Strangeness mixing and quenching in the Nambu-Jona-Lasinio model, *Nucl. Phys.* **B308**, 753 (1988).
- [62] S. Klimt, M. F. M. Lutz, U. Vogl, and W. Weise, Generalized Nambu-Jona-Lasinio model. Part I. Mesonic modes, *Nucl. Phys.* **A516**, 429 (1990).
- [63] U. Vogl and W. Weise, The Nambu and Jona Lasinio model: its implications for hadrons and nuclei, *Prog. Part. Nucl. Phys.* **27**, 195 (1991).
- [64] M. F. M. Lutz, S. Klimt, and W. Weise, Meson properties at finite temperature and baryon density, *Nucl. Phys.* **A542**, 521 (1992).
- [65] S. P. Klevansky, The Nambu-Jona-Lasinio model of quantum chromodynamics, *Rev. Mod. Phys.* **64**, 649 (1992).
- [66] T. Hatsuda and T. Kunihiro, QCD phenomenology based on a chiral effective lagrangian, *Phys. Rep.* **247**, 221 (1994).
- [67] M. Buballa, NJL model analysis of quark matter at large density, *Phys. Rep.* **407**, 205 (2005).
- [68] G. 't Hooft, Computation of the quantum effects due to a four-dimensional pseudoparticle, *Phys. Rev. D* **14**, 3432 (1976); **18**, 2199 (1978).
- [69] M. A. Shifman, A. I. Vainshtein, and V. I. Zakharov, Instanton density in a theory with massless quarks, *Nucl. Phys.* **B163**, 46 (1980).
- [70] C. Vafa and E. Witten, Parity Conservation in QCD, *Phys. Rev. Lett.* **53**, 535 (1984).